Calculation of nearly singular boundary element integrals in thin structures using an improved exponential transformation

Guizhong Xie[1], Jianming Zhang [1, 2], Cheng Huang[1], Chenjun Lu [1], Guangyao Li[1]

Abstract: In this work, an improved exponential transformation is presented for nearly singular boundary element integrals in problems of thin structures. Accurate evaluation of nearly singular integrals is an important issue in the implementation of boundary element method (BEM) for thin structures. In this paper, the exponential transformation, which was firstly developed to evaluate nearly singular integrals arising in 2D BEM, is extended into 3D BEM to deal with nearly singular integrals. Firstly, a novel (α, β) coordinate system is introduced. Then, the conventional distance function is modified into a new form in (α, β) coordinate system. Based on the refined distance function, finally, an improved exponential transformation is employed in the new coordinate system. Furthermore, to perform integrations on irregular elements, an adaptive integration scheme considering both the shape of element and the projection point associated with the improved transformation is proposed. Numerical examples are presented to verify the proposed method. Results demonstrate the accuracy and efficiency of our method. Moreover, the accuracy of our method is less sensitive to the position of the projection point than that of the traditional methods.

Keywords: nearly singular integrals; boundary element method; boundary face method; the exponential transformation

1. INTRODUCTION

Near singularities are involved in many boundary element method (BEM) analyses of engineering problems, such as problems on thin shell-like structures [Krishnasamy *et al* (1994); Liu (1998)],

[1] State Key Laboratory of Advanced Design and Manufacturing for Vehicle Body, College of Mechanical and Vehicle Engineering, Hunan University, Changsha 410082, China

[2] Corresponding author.   Tel: +86-731-88823061 Fax: +86-731-88823051
Email: zhangjm@hnu.edu.cn

the crack problems [Dirgantara *et al* (2000)], the contact problems [Aliabadi (2000)], as well as the sensitivity problems [Zhang D *et al* (1999)]. Accurate and efficient evaluation of nearly singular integrals with various kernel functions of the type $O(1/r^\chi)$ is crucial for successful implementation of boundary type numerical methods based on boundary integral equations (BIEs), such as boundary element method (BEM), boundary face method (BFM) [Zhang JM *et al* (2009); F.L. Zhou *et al* (2013)]. A near singularity arises when a source point is close to but not on the integration elements. Although those integrals are actually regular in nature, they can't be evaluated accurately by the standard Gaussian quadrature. This is because, the denominator r, the distance between the source and the field point, is close to zero but not zero. The difficulty encountered in the numerical evaluation mainly results from the fact that the integrands of nearly singular integrals vary drastically with respect to the distance r. Effective computation of nearly singular integrals has received intensive attention in recent years [Atluri *et al* (2003), (2004), (2006)]. Various numerical techniques have been developed to remove the near singularities, such as global regularization [Sladek *et al* (1993); Liu (1999); Zhang J.M. *et al* (2001), (2004)], semi-analytical or analytical integral formulas [Niu *et al* (2005); Zhou *et al* (2008)], the sinh transformation [Johnston *et al* (2005)], polynomial transformation [Telles (1987)], adaptive subdivision method [Gao (2000); Zhang J.M. *et al* (2009)], distance transformation technique [Ma *et al* (2001), (2001); Qin *et al* (2011)], the PART method [Hayami (1994), (2005)], and the exponential transformation [Xie *et al* (2011), (2013); Zhang YM *et al* (2009), (2010)]. However, the idea behind those methods for evaluating nearly singular integrals is to shift the integration points close to the projection point. The results of those methods are sensitive to the position of the projection point. Moreover, if irregular elements are used, the accuracy of these methods will be influenced a lot. Among those techniques, the exponential transformation technique seems to be a more promising method for dealing with different orders of nearly singular integrals. However, the transformation is only limited to 2D boundary element. In this paper, we develop the exponential transformation technique for nearly singular integrals in 3D boundary element method.

In our method, first a new local coordinate system described by (α, β) is introduced. This system is similar to the polar system, but its implementation is simpler than the polar system and also performs efficiently. Then the conventional distance function is modified into a new form in

(α, β) coordinate system. Based on the modified distance function, the exponential transformation in Refs. [Xie *et al* (2011), (2013), Zhang Y.M. *et al* (2009), (2010)] can be developed to 3D BEM in (α, β) coordinate system. To perform integrations on irregular elements, the element subdivision technique considering both the element shape and the positions of the project point is employed in combination with the improved transformation. Although the element subdivision technique is employed, the computational cost is reduced dramatically compared with the conventional element subdivision techniques [Gao (2000); Zhang J.M. *et al* (2009)]. With our method, the boundary nearly singular integrals of regular or irregular elements can be accurately and effectively calculated. Numerical examples are presented to validate the proposed method. Results demonstrate the accuracy and efficiency of our method. Moreover, our method is less sensitive to the position of the project point than the conventional methods.

This paper is organized as follows. The general form of nearly singular integrals is described in Section 2. Section 3 briefly reviews the distance function in polar coordinate system and then the distance function is constructed in (α, β) coordinate system in a new form. In Section 4, the transformations for nearly singular integrals are presented and the element subdivision technique is introduced. Numerical examples are given in Section 5. The paper ends with conclusions in Section 6.

2. GENERAL DESCRIPTIONS

In this section, we will give a general form of nearly singular integrals on 3D boundary elements. First we consider the boundary integral equation for 3D elasticity problems. The well-known self-regular BIE for elasticity problems in 3-D is

$$0 = \int_{\Gamma} (u_j(\mathbf{s}) - u_j(\mathbf{y})) T_{ij}(\mathbf{s}, \mathbf{y}) d\Gamma - \int_{\Gamma} t_j(\mathbf{s}) U_{ij}(\mathbf{s}, \mathbf{y}) d\Gamma \qquad (1)$$

where $\mathbf{s}$ and $\mathbf{y}$ represent the field point and the source point in the BEM, with components s_i and y_i, *i=1,2,3*, respectively.

Eq. (1) is discretized on the boundary Γ by boundary elements $\Gamma_e (e = 1 \sim N)$ defined by interpolation functions. The integral kernels of Eq. (1) become nearly singular when the distance between the source point and integration element is very small compared to the size of integration element. And the integrals in Eq. (1) become nearly singular with different orders, namely,

$U_{ij}(\mathbf{s}, \mathbf{y})$ with near weak singularity, and $T_{ij}(\mathbf{s}, \mathbf{y})$ with near strong singularity. In this paper, we develop the exponential transformation method for various boundary integrals with near singularities of different orders. The new method is detailed in following sections. For the sake of clarity and brevity, we take following integrals as a general form to discuss:

$$I = \int_S \frac{f(\mathbf{x}, \mathbf{y})}{r^l} dS, \quad l = 1, 2, 3 \quad r = \|\mathbf{x} - \mathbf{y}\|_2 \tag{2}$$

where f is a smooth function, $\mathbf{x}$ and $\mathbf{y}$ represent the field point and the source point in BEM, with components x_i and y_i, respectively. S represents the boundary element. We assume that the source point is close to S, but not on it.

3. CONSTRUCTION OF NEW DISTANCE FUNCTION

3.1 The conventional distance function in polar coordinate

In this section, we will briefly review the distance function [Ma *et al* (2001), (2001); Qin *et al* 2011)].
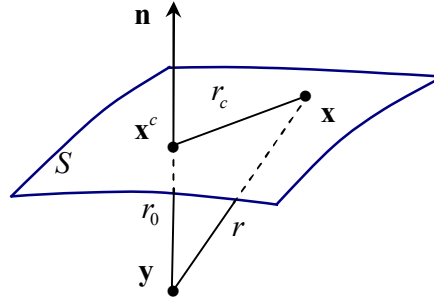

Figure 1: The minimum distance r_0, from the source point $\mathbf{x^c}$ to the 3D surface element

As shown in Fig.1, employing the first-order Taylor expansion in the neighborhood of the projection point, we have:

$$
\begin{aligned}
x_k - y_k &= x_k - x_k^c + x_k^c - y_k \\
&= \frac{\partial x_k}{\partial t_1}\bigg|_{\substack{t_1=c_1 \\ t_2=c_2}} (t_1 - c_1) + \frac{\partial x_k}{\partial t_2}\bigg|_{\substack{t_1=c_1 \\ t_2=c_2}} (t_2 - c_2) + r_0 n_k(c_1, c_2) + O(\rho^2) \\
&= \rho A_k(\theta) + r_0 n_k(c_1, c_2) + O(\rho^2)
\end{aligned}
\tag{3}
$$

where (c_1, c_2) are the coordinates of the projection point in the local system (t_1, t_2),

$\rho = \sqrt{(t_1 - c_1)^2 + (t_2 - c_2)^2}$ and $r_0 = \left\| \mathbf{x}^c - \mathbf{y} \right\|$ which is the minimum distance from the source point to the element. n_k represents the component of the unit outward direction to the surface boundary and

$$A_k(\theta) = \frac{\partial x_k}{\partial t_1}\bigg|_{\substack{t_1=c_1 \\ t_2=c_2}} \cos\theta + \frac{\partial x_k}{\partial t_2}\bigg|_{\substack{t_1=c_1 \\ t_2=c_2}} \sin\theta \tag{4}$$

The distance function is expressed as follows:

$$r^2 = (x_k - y_k)(x_k - y_k) = A_k^2(\theta)\rho^2 + r_0^2 + O(\rho^3) \tag{5a}$$

$$r = \sqrt{A_k^2(\theta)\rho^2 + r_0^2 + O(\rho^3)} \tag{5b}$$

Using Eq. (5a) and Eq. (5b), Eq. (2) can be written as:

$$I = \int_\Gamma \frac{f(\mathbf{x},\mathbf{y})}{r^l}d\Gamma = \sum_m \int_{\theta_m}^{\theta_{m+1}} \int_0^{\rho(\theta)} \frac{g(\rho,\theta)}{(\rho^2 + \omega^2(\theta))^{l/2}}d\rho d\theta \tag{6}$$

where $\omega(\theta) = \dfrac{r_0}{A(\theta)}$, $A(\theta) = \sqrt{A_k(\theta)A_k(\theta)}$, and $g(\rho,\theta)$ is a smooth function.

3.2 The conventional distance function in (α,β) coordinate

To construct the local (α,β) system shown in Fig. 2, the following mapping scheme which is used for calculating weakly singular integrals [Zhang J.M. *et al* (2009)] is introduced:
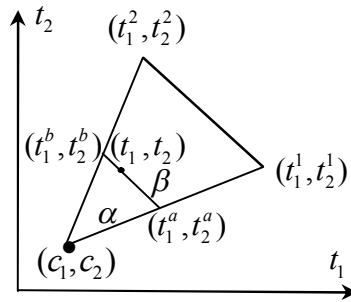

Figure 2: new system (α,β)

It is different to obtain the coordinates t_1 and t_2 in (α,β) system compared with the polar coordinate system above, which can be written as:

$$\begin{cases} t_1 = c_1 + (t_1^1 - c_1)\alpha + (t_1^2 - t_1^1)\alpha\beta \\ t_2 = c_2 + (t_2^1 - c_2)\alpha + (t_2^2 - t_2^1)\alpha\beta \end{cases} \quad \alpha,\beta \in [0,1] \tag{7}$$

The Jacobian for the transformation from (t_1, t_2) system to (α, β) system is αS_Δ, where

$$S_\Delta = \left| t_1^1 t_2^2 + t_1^2 c_2 + c_1 t_2^1 - t_1^2 t_2^1 - c_1 t_2^2 - t_1^1 c_2 \right| \tag{8}$$

Using Eq. (7) ,we can get:

$$
\begin{aligned}
x_k - y_k &= x_k - x_k^c + x_k^c - y_k \\
&= \left.\frac{\partial x_k}{\partial t_1}\right|_{\substack{t_1=c_1 \\ t_2=c_2}} (t_1 - c_1) + \left.\frac{\partial x_k}{\partial t_2}\right|_{\substack{t_1=c_1 \\ t_2=c_2}} (t_1 - c_2) + r_0 n_k (c_1, c_2) + O(\alpha^2) \\
&= \alpha A_k(\beta) + r_0 n_k(c_1, c_2) + O(\alpha^2)
\end{aligned}
\tag{9}
$$

where

$$A_k(\beta) = \left.\frac{\partial x_k}{\partial t_1}\right|_{\substack{t_1=c_1 \\ t_2=c_2}} \left[(t_1^1 - t_1^0) + (t_1^2 - t_1^1)\beta \right] + \left.\frac{\partial x_k}{\partial t_2}\right|_{\substack{t_1=c_1 \\ t_2=c_2}} \left[(t_2^1 - t_2^0) + (t_2^2 - t_2^1)\beta \right] \tag{10}$$

Using Eqs. (7) - (10), we can easily obtain the distance function in a new form:

$$r^2 = (x_k - y_k)(x_k - y_k) = A_k^2(\beta)\alpha^2 + r_0^2 + O(\alpha^3) \tag{11a}$$

$$r = \sqrt{A_k^2(\beta)\alpha^2 + r_0^2 + O(\alpha^3)} \tag{11b}$$

Using Eqs. (11a) - (11b), Eq. (2) can be written as:

$$I = \int_\Gamma \frac{f(\mathbf{x}, \mathbf{y})}{r^l} d\Gamma = \sum_m \int_0^1 \int_0^1 \frac{g(\alpha, \beta)}{(\alpha^2 + \lambda^2(\beta))^{l/2}} d\alpha d\beta \tag{12}$$

where $\lambda(\beta) = \dfrac{r_0}{A(\beta)}$, $A(\beta) = \sqrt{A_k(\beta)A_k(\beta)}$, and $g(\alpha, \beta)$ is a smooth function.

3.3 Improved distance function in (α, β) coordinate system

The conventional distance function in (α, β) coordinate system has been reviewed in Section 3.2. However, as illustrated in Fig. 3, if the projection point is not the ideal point, the line with end points $\mathbf{x}^c$ and $\mathbf{y}$ is not perpendicular to the tangential plane through $\mathbf{x}^c$.
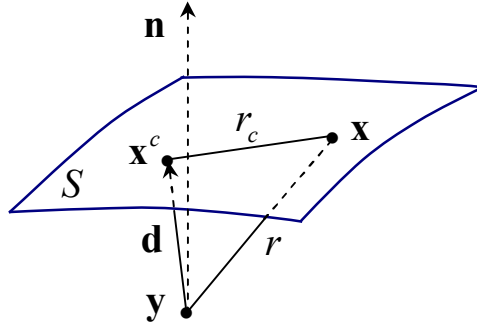
Figure 3: The projection point is not the ideal point

Using Eq. (9) and Eq. (11a), the real distance between the source point and the field points can be written as:

$$r^2 = (x_k - y_k)(x_k - y_k) = a\left[(\alpha + \frac{b}{2a})^2 + \frac{r_0^2}{a} - (\frac{b}{2a})^2 + O(\alpha^3)\right] \tag{13a}$$

where $a = A_k^2(\beta) > 0$, $b = 2d_k A_k(\beta)$, $r_0^2 = |\mathbf{d}|^2$

The following distance function can be given as:

$$r = \sqrt{a}\sqrt{\left[(\alpha + \frac{b}{2a})^2 + \delta^2 + O(\alpha^3)\right]} \tag{13b}$$

where $\delta^2 = \frac{r_0^2}{a} - (\frac{b}{2a})^2$

Using Eq. (13a) and Eq. (13b), Eq. (2) can be written as:

$$I = \int_\Gamma \frac{f(\mathbf{x},\mathbf{y})}{r^l} d\Gamma = \sum_m \int_0^1\int_0^1 \frac{g(\alpha,\beta)}{[(\alpha + \frac{b}{2a})^2 + \delta^2]^{l/2}} d\alpha d\beta \tag{14}$$

where $\delta^2 = \frac{r_0^2}{a} - (\frac{b}{2a})^2$, $A(\beta) = \sqrt{A_k(\beta)A_k(\beta)}$, and $g(\alpha,\beta)$ is a smooth function.

In this section, we obtain the distance function in a new form in the (α,β) coordinate system. It is should be noted that if the project point is coincide with ideal projection point, Eq. (14) is similar to Eq. (12). In next section, we will construct the improved exponential transformation based on the refined distance function (13b).

4. Improved transformation and element subdivision technique

4.1 Improved exponential transformation

In this section, we will give the improved transformation considering the modified distance

function. As observed Eq. (12) and Eq. (14), the near singularity is essentially related to the radial variable α .

From Eq. (12), we only consider the radial variable integral which depicts near singularity in the Eq. (12), as follows:

$$I_2 = \int_0^1 \frac{g(\alpha,\beta)}{(\alpha^2 + \lambda^2(\beta))^{l/2}} d\alpha \tag{15}$$

The following exponential transformation is given:

$$\alpha = \lambda(\beta)(e^{k(1+\eta)} - 1),\ \eta \in [-1,1],\ \ k = \ln\sqrt{1 + 1/\lambda(\beta)} \tag{16}$$

Substituting Eq. (16) into Eq. (15), we have:

$$I_2 = \int_0^1 \frac{g(\alpha,\beta)}{(\alpha^2 + \lambda^2(\beta))^{l/2}} d\alpha = \int_{-1}^1 \frac{k\lambda(\beta)e^{k(1+\eta)}g(\rho,\theta)}{\lambda^l(\beta)((e^{k(1+\eta)} - 1)^2 + 1)^l} d\eta \tag{17}$$

It is should be noted that the exponential transformation in (α,β) coordinate system is analogous to the polar coordinate system. However, the (α,β) system is much simpler than the polar system. This is because both α and β are constrained to the interval [0, 1] in each triangle, and there is no need to calculate their spans. On the contrary, the spans for both ρ and θ in the polar system are needed to be determined complicatedly in each triangle for different types of boundary elements.

Then from Eq. (14), we only consider the radial variable integral which depicts near singularity in the Eq. (14), as follows:

$$I_2 = \int_0^1 \frac{g(\alpha,\beta)}{[(\alpha + \frac{b}{2a})^2 + \delta^2]^{l/2}} d\alpha \tag{18}$$

The following exponential transformation is given:

$$\alpha = \delta(e^{k(1+\eta)} - 1 + \frac{b}{2a\delta}) - \frac{b}{2a}\ \eta \in [-1,1],\ \ k = \ln\sqrt{1 + 1/\delta} \tag{19}$$

Note that if the projection point is the ideal projection point, Eq. (19) is similar to Eq. (16). Moreover, the form of Eq. (19) is analogous to that of Eq. (16). With the exponential transformation above, the integrals with near weak singularity or near strong singularity can be

accurately calculated. It should be noted that we still use the exact *r* instead of the approximate r in Eq. (14). So the nearly singular kernels are not changed into other forms.

4.2 Exponential transformation in combination with element subdivision

In this section, we define the elements of which the length and width ratio is much larger than 1, as irregular elements, as shown in Fig. 4(b). If we directly subdivide the initial irregular elements into several triangles, the shape of triangles may be poor shown in Fig. 5(a) - Fig. 5(f) and nearly singular integrals on the integration patches may be not accurately calculated. Thus element subdivision is indispensible for treating the nearly singular integrals in the 3D cases as in Refs. [Ma *et al* (2001), (2002); Qin *et al* (2011)], especially for irregular elements.
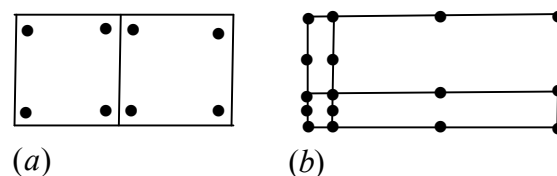

(*a*)   (*b*)

Figure 4: Two types of the element: (a) Discontinuous elements (b) Element sizes quite are

different

In this section, we subdivide an integration element in a suitable pattern considering both the shape of the element and the position of the projection point in the element, and adaptive integration scheme based on element subdivision to calculate integrals is employed just as a combination for the improved exponential transformation. The element subdivision technique is similar to that discussed in Refs. [Zhang J.M. *et al* (2009); Qin *et al* (2013)], but there are some improvements in our work.

Note that although the shape of the original quadrilateral is fine, the quality of four sub-triangles may be poor. The quality of the sub-triangle depends on the position of $\mathbf{x^c}$ (the projection point) (see Fig. 5 (*a*)).
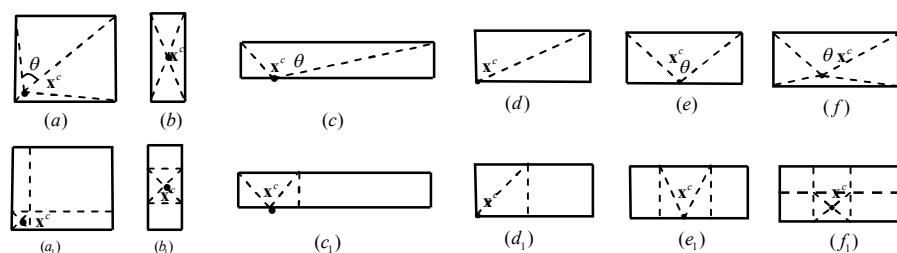
Figure 5: Subdivisions of quadrilateral element depending on the position of the projection point

Obtaining triangles of fine shape seems more difficult by direct subdivision for initial irregular elements as shown in Fig. 5(*e*) even $\mathbf{x^c}$ is located at the element center. If the angle denoted by, Fig. 5(*b*) – 5(*f*) between two lines with end point $\mathbf{x^c}$ in each triangle is larger by a certain value $2\pi/3$ and even tends to π, numerical results will become less accurate.

To solve the troubles described above, we have developed an adaptive subdivision for an arbitrary quadrilateral element. The original element is divided into several triangles and additional quadrangles, which is different from these shown in Fig. 5 (*a*)-(*f*). The adaptive subdivision consists of three main steps described briefly as follows:

First, compute the distances in the real-world-coordinate system from $\mathbf{x^c}$ to each edge of the element and obtain the minimum distance *d*.

Then, based on d, we construct a box defined in the parametric system, and with square shape in the real- world -coordinate system to well cover $\mathbf{x^c}$ e.

Finally, triangles are constructed from the box and additional quadrangles are created outside the box in the element.

Applying the strategy above, adaptive subdivisions for the elements in Fig. 5 with suitable patterns are shown in Fig. 5(a_1)-(f_1). For each triangle, the nearly singular integrals are calculated by the scheme discussed in Section 4.1. However, for each quadrangle, nearly singular integrals will arise but not be severe, which can be calculated by adaptive integration scheme based on the element subdivision technique discussed in Refs. [Zhang J.M. *et al* (2009)].

It should be noted that, although the element subdivision technique is adopted, the computational cost is reduced dramatically compared with the conventional subdivision technique to compute nearly singular integrals on the whole element. This is because the integrals on the local region of the element, which is more close to the source point, are calculated by the improved exponential transformation technique. Thus a large number of integration points concentrated near the projection point are avoided.

5. NUMERICAL EXAMPLES

Example 1: A spherical surface element

This example considers nearly singular integrals on a curved surface element. The curved surface element is presented in parametric form by a local spherical polar system, and element of this kind is named as spherical surface element here which is usually used in BFM [Zhang JM *et al* (2009); F.L. Zhou *et al* (2013)]. The element's geometric parameters are given as follows: $\theta \in [0, \pi/4]$,

$\varphi \in [\pi/6, 5\pi/12]$ and the sphere radius (r) is set to 0.1, with center $(0,0,0)$. The projection point of the given source point is located at the center of the element. In this example, we consider the high order shape function. The shape function is expressed as follows:

$$\Phi = (-1 - t_1 - t_2)(1 - t_1)(1 - t_2)/4 \qquad (20)$$

The *ratio* is the ratio of the distance between the source point and the projection point to the sphere radius. The Young's modulus is 1 and the Poisson's ratio is 0.25. Various integrals with kernel U_{11} are computed by our method and Ma's method [Ma *et al* (2001), (2001)] and the relative errors are listed in Table 1. Various integrals with kenel T_{11} are computed by our method and the relative errors are listed in Table 2. From Table 1, it can be noted that when *ratio* >0.01, the Ma's method produces superior results to our method. However, when *ratio* becomes smaller, the efficiency of the Ma's method decreases, and the efficiency of our method remains nearly constant. Compared with Ma's method, the proposed method is effective for nearly singular integrals with kernel U_{11}. From Table 2, it can be found that for integrals with kernel T_{11}, the relative errors increase up to 10^{-4}. The results denote that our method can be directly used for the curved surface element with high order shape functions in BEM.

Table 1 Relative errors of our method for integrals with kernel U_{11} by our method compared with Ma's method

integrals with kernel U_{11} and shape function, x^c =(0.5, 0.5)		
ratio	*Exact solution*	*Our method*	*Ma's method*
10^{-1}	-0.00327870335	7.46E-10	1.38E-08
10^{-2}	-0.00507743182	2.24E-10	5.30E-08
10^{-3}	-0.00531026259	5.98E-07	2.62E-08
10^{-4}	-0.00533414094	3.30E-06	6.15E-07
10^{-5}	-0.00533653480	4.31E-05	3.52E-07

Table 2 Relative errors of our method for integrals with kernel T_{11}

integrals with kernel U_{11} and shape function, x^c =(0.5, 0.5)		
ratio	*Exact solution*	*Our method*
10^{-1}	-0.0642775962	1.21E-08

10^{-2}	-0.1301736177	3.20E-06
10^{-3}	-0.1388015889	1.96E-06
10^{-4}	-0.13968571546	2.15E-05
10^{-5}	-0.13977434165	6.34E-04

In this example, we also study the influence of the projection point on our method when the source point is fixed. In each case, the *ratio* is fixed at 0.01, and the projection point **P** is determined by an offset parameter $k, 0 \le k \le 0.1$, using the following equation :

$$\mathbf{p} = \mathbf{x}^c - k\mathbf{x}^c \qquad (21)$$

where $\mathbf{x}^c$ is the ideal projection point at the centre of the element with coordinates (0, 0) in local (t_1, t_2) system if we constrain both t_1 and t_2 in [-1, 1]. Given a set of values of k, all computations have been performed with our method using Eq. (14) and distance transformation [Ma *et al* (2001), (2001)], respectively. The reference values are obtained by adaptive element subdivisions [Zhang J.M (2009)]. As seen in Table 3, it is obvious that, the results obtained by Eq. (14) are in good agreement with the reference values even the offset parameter k increases up to 10%, and the relative errors are very small with the order less than 10^{-4}.

Table 3 Relative errors of our method for integrals with kernel U_{11} by our method compared with Ma's method as the offset parameter k varies

integrals with kernel U_{11} and shape function, $\mathbf{x}^c$ =(0.5, 0.5) ratio=0.01

k(%)	Exact solution	Our method	Ma's method
1	-0.00507743182	8.00e-06	5.51e-04
3	-0.00507743182	5.70e-04	9.6e-03
5	-0.00507743182	3.15e-05	1.90e-03
7	-0.00507743182	4.25e-06	wrong
9	-0.00507743182	5.63e-06	wrong

It is should be noted that although in most cases the projection point coincides with the ideal projection point, the special cases of the offset projection point are also considered in this paper. In our implementation, the improved exponential transformation is applied for evaluation of the nearly singular integrals arising in 3D boundary elements. This is because the accuracy of the results is less sensitive to the position of the project point.

Example 2: ***A thin plate problem***

The geometry, boundary conditions, and the model for the problem are shown in Fig. 6. We assume the thickness is 0.01. The Young's modulus is 1 and the Poisson's ratio is 0.25. In order to assess the accuracy of the present method, boundary conditions of Dirichlet type are imposed on all faces corresponding to quadratic exact solutions. And the solutions are as follows:

$$\begin{cases} u_x = -2x^2 + 3y^2 + 3z^2 \\ u_y = 3x^2 - 2y^2 + 3z^2 \\ u_z = 3x^2 + 3y^2 - 2z^2 \end{cases} \tag{22}$$

The BEM model employed in this example is depicted in Fig. 6. It consists of 240 8-node quadrilateral elements with a total of 770 nodes. For side surfaces, 8-node discontinuous quadrilateral elements are used. As illustrated in Fig. 6, the elements are slender elements in the side surfaces. To evaluate the nearly singular integrals, the improved transformation combined with the element subdivision technique is applied. The sample points are distributed on the boundary. The boundary sample points are well-distributed on isoparametric line segment from (2, -2) to (-2, 2) in the parametric space of the surface (y=0.005). Results at the sample points are illustrated in Fig. 7.

As shown in Fig. 7, with the proposed method, the near singularities are removed efficiently and accurate numerical results have been obtained. The slender element, of which the length and width ratio is larger than 10, is applied for long and narrow surfaces in this example. In our method, however, the accuracy is not influenced by elements with poor quality. The maximum error is within 1 percent.
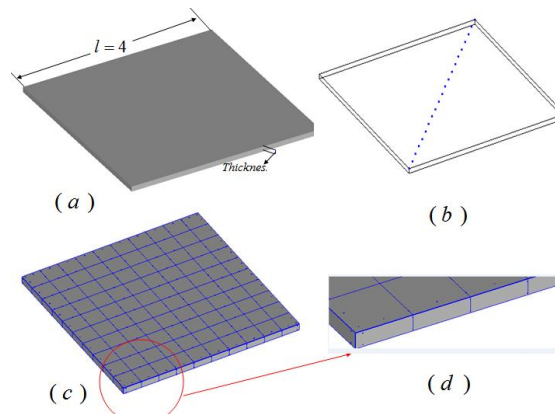

Figure 6: (*a*) A thin plate (*b*) Sample points (*c*) Discretization of the thin plate (*d*) Slender elements
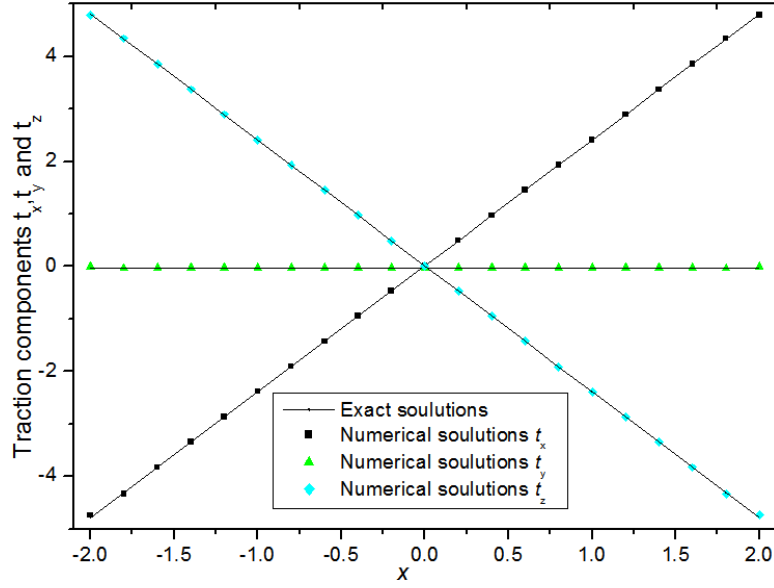
Figure 7: Results at the sample points

Example 3:   Thin cylindrical shell with fixed ends subjected to constant internal pressure

This problem setup and a radial displacement profile are shown in Fig. 8. Note that the fixed ends create boundary layers which are difficult to capture with finite element methods. The exact shell theory solution is given in Ref. [Hughes (2005)], for plane stress and provided as a reference solution as below:

$$u(x) = -\frac{PR^2}{Et}(1 - C_1 \sin \beta x \sinh \beta x - C_2 \cos \beta x \cosh \beta x) \quad x \in (-L/2, L/2) \tag{23}$$

where $C_1 = \dfrac{\sin \alpha \cosh \alpha - \cos \alpha \sinh \alpha}{\sinh \alpha \cosh \alpha + \sin \alpha \cos \alpha}$, $C_2 = \dfrac{\cos \alpha \sinh \alpha + \sin \alpha \cosh \alpha}{\sinh \alpha \cosh \alpha + \sin \alpha \cos \alpha}$

The sample points are uniformly distributed on the line segment which has end points at (*-2.01, 0, -4.99*) and (*-2.01, 0, 4.99*). The Young's modulus is *1800* and the Poisson's ratio is *0.25*. The BFM model with *448* 8-node quadrilateral elements and the total number of nodes is *1454*. 16 slender elements are also employed in this example. Results at the sample points are illustrated in Fig. 9.

$$R = 2.0$$
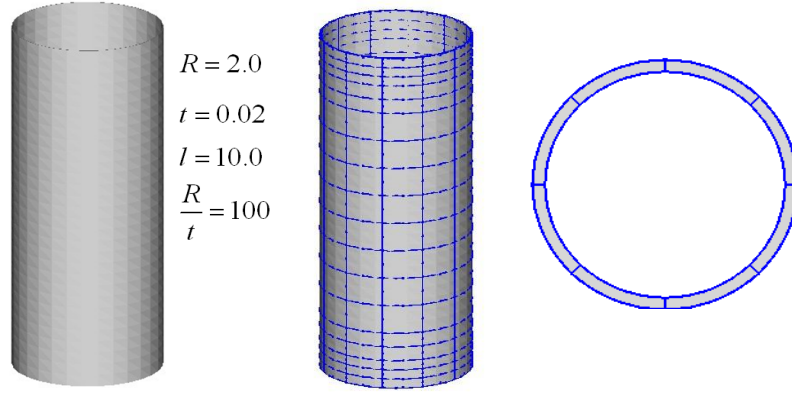$$t = 0.02$$
$$l = 10.0$$
$$\frac{R}{t} = 100$$

Figure 8: Thin cylindrical shell, surface meshes, and the meshes of the end face
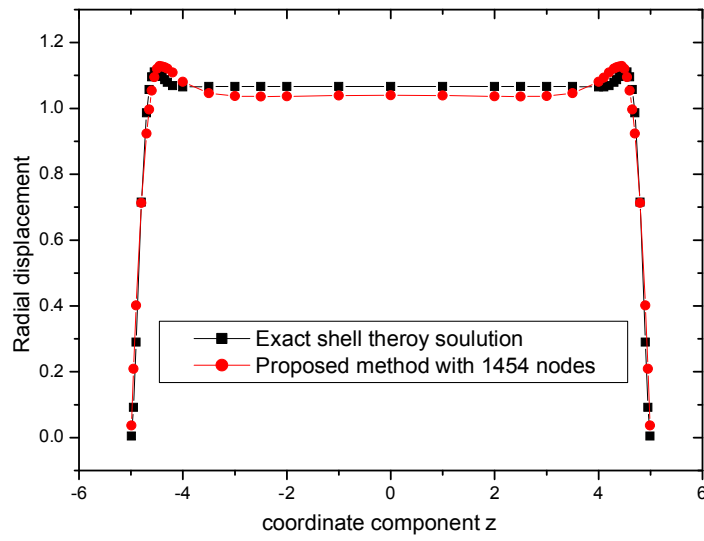

Figure 9: Numerical radial displacement compared with the shell theory solution

From Fig. 9, although the results are not that accurate, it can be seen that the numerical radial displacement profile captures the boundary layers and picks up the plateau very well. Compared with FEM, the plate and shell theories based on various assumptions about the geometry are not needed in BEM. Moreover, compared with the method in [Hughes (2005)], no solid element is required in BEM.

6. CONCLUSIONS

This paper presented an improved exponential transformation for nearly singular integrals which appears in the application of BEM for thin structures. By applying the proposed transformation in the BEM, near singular integrals arising in the 3D BEM can be accurately calculated. Furthermore, results obtained by the proposed method are less sensitive to the location

of the projection point than that obtained by the traditional method.

To perform integration on irregular elements, an adaptive integration scheme considering the element shape and the projection point in combination with the improved transformation has been introduced. Numerical examples compared with other methods have been presented to verify the proposed method. Results demonstrate the accuracy and efficiency of our method. Extending our method for nearly hypersingular integrals is ongoing.

REFERENCES

Aliabadi, M.H.; Martin, D. (2000): Boundary element hypersingular formulation for elastoplastic contact problems. *International Journal for Numerical Methods in Engineering*, vol. 48, no. 7, pp. 995-1014.

Atluri, S.N.; Han, Z.D.; Shen, S. (2003): Meshless Local Petrov-Galerkin (MLPG) approaches for weakly-singular traction & displacement boundary integral equations, *CMES: Computer Modeling in Engineering & Science*, vol. 4, no. 5, pp. 507-517.

Atluri, S.N. (2004): The Meshless Local Petrov-Galerkin (MLPG) Method for Domain & Boundary Discretizations, Tech Science Press, 665 pages.

Atluri, S.N.; Liu, H.T.; Han, Z.D. (2006a): Meshless Local Petrov-Galerkin (MLPG) Mixed Collocation Method for Elasticity Problems, *CMES: Computer Modeling in Engineering & Sciences*, vol. 14, no. 3, pp. 141-152.

Atluri, S.N.; Liu, H.T.; Han, Z.D. (2006b): Meshless Local Petrov-Galerkin (MLPG) Mixed Finite Difference Method for Solid Mechanics, *CMES: Computer Modeling in Engineering & Sciences*, vol. 15, no. 1, pp. 1-16.

Cruse, T. A.; Aithal, R. (1993): Non-singular boundary integral equation implementation. *International journal for numerical methods in engineering*, vol. 36, no. 2, pp. 237-254.

Chen, H. B.; Lu, P.; Huang, M. G.; Williams, F. W. (1998): An effective method for finding values on and near boundaries in the elastic BEM. *Computers & structures*, vol. 69, no. 4, pp. 421-431.

Dirgantara, T.; Aliabadi, M. H. (2000): Crack growth analysis of plates loaded by bending and

tension using dual boundary element method. *International journal of fracture*, vol. 105, no. 1, pp. 27-47.

F.L. Zhou.; G.Z. Xie.; J.M. Zhang.; X.S. Zheng. (2013): Transient heat conduction analysis of solids with small open-ended tubular cavities by boundary face method. *Engineering Analysis with Boundary Elements*, vol. 37, no. 3, pp. 542-550.

Gao, X. W.; Davies, T. G. (2000): Adaptive integration in elasto-plastic boundary element analysis. *Journal of the Chinese institute of engineers*, vol. 23, no .3, pp. 349-356.

Hayami, K.; Matsumoto, H. (1994): A numerical quadrature for nearly singular boundary element integrals. *Engineering Analysis with Boundary Elements*, vol.13, no. 2, pp. 143-154.

Hayami, K. (2005): Variable transformations for nearly singular integrals in the boundary element method. *Publications of the Research Institute for Mathematical Sciences*, vol. 41, no. 4, pp. 821-842.

Hughes, T. J.; Cottrell, J. A.; Bazilevs, Y. (2005): Isogeometric analysis: CAD, finite elements, NURBS, exact geometry and mesh refinement. *Computer methods in applied mechanics and engineering*, vol. 194, no. 39, pp. 4135-4195.

Johnston, P. R.; Elliott, D. (2005): A sinh transformation for evaluating nearly singular boundary element integrals. *International journal for numerical methods in engineering*, vol. 62, no. 4, pp. 564-578.

Johnston, B. M.; Johnston, P. R.; Elliott, D. (2007): A sinh transformation for evaluating two‑dimensional nearly singular boundary element integrals. *International journal for numerical methods in engineering*,vol. 69, no.7, pp. 1460-1479.

Krishnasamy, G.; Rizzo, F. J.; Liu, Y. (1994): Boundary integral equations for thin bodies. *International Journal for Numerical Methods in Engineering*, vol. 37, no. 1, pp. 107-121.

Liu, Y. J. (1998): Analysis of shell-like structures by the boundary element method based on 3-D elasticity: formulation and verification. *International Journal for Numerical Methods in Engineering*, vol. 41, no. 3, pp. 541-558.

Liu, Y. J.; Rudolphi, T. J. (1999): New identities for fundamental solutions and their applications to non-singular boundary element formulations. *Computational mechanics*, vol. 24, no. 4, pp. 286-292.

Ma, H.; Kamiya, N. (2002): A general algorithm for the numerical evaluation of nearly singular

boundary integrals of various orders for two-and three-dimensional elasticity. *Computational Mechanics*, vol. 29, no. 4, pp. 277-288.

Ma, H.; Kamiya, N. (2001): A general algorithm for accurate computation of field variables and its derivatives near the boundary in BEM. *Engineering analysis with boundary elements*, vol. 25, no. 10, pp. 833-841.

Ma, H.; Kamiya, N. (2002): Distance transformation for the numerical evaluation of near singular boundary integrals with various kernels in boundary element method. *Engineering analysis with boundary elements*, vol. 26, no. 4, pp. 329-339.

Niu, Z.; Wendland, W. L.; Wang, X.; Zhou, H. (2005): A semi-analytical algorithm for the evaluation of the nearly singular integrals in three-dimensional boundary element methods. *Computer methods in applied mechanics and engineering*, vol. 194, no. 9, pp. 1057-1074.

Qin, X.; Zhang, J.; Xie, G.; Zhou, F.; Li, G. (2011). A general algorithm for the numerical evaluation of nearly singular integrals on 3D boundary element. *Journal of computational and applied mathematics*, vol. 235, no. 14, pp. 4174-4186.

Sladek, V.; Sladek, J.; Tanaka, M. (1993): Regularization of hypersingular and nearly singular integrals in the potential theory and elasticity. *International Journal for Numerical Methods in Engineering*, vol. 36, no. 10, pp. 1609-1628.

Telles, J.C.F. (1987): A self adaptive coordinate transformation for efficient numerical evaluations of general boundary element integrals, *International Journal for Numerical Methods in Engineering*, vol. 24, no. 5, pp. 959-973.

Xie, G.; Zhang, J.; Qin, X.; Li, G. (2011): New variable transformations for evaluating nearly singular integrals in 2D boundary element method. *Engineering Analysis with Boundary Elements*, vol. 35, no. 6, pp. 811-817.

Xie, G., Zhou, F., Zhang, J., Zheng, X., & Huang, C. (2013): New variable transformations for evaluating nearly singular integrals in 3D boundary element method. *Engineering Analysis with Boundary Elements*, vol. 37, no. 9, pp. 1169-1178.

Zhang, D.; Rizzo, F. J.; Rudolphi, Y. J. (1999): Stress intensity sensitivities via hypersingular boundary element integral equations. *Computational Mechanics*, vol. 23, pp. 389-396.

Zhou, H.; Niu, Z.; Cheng, C.; Guan, Z. (2008)：Analytical integral algorithm applied to boundary layer effect and thin body effect in BEM for anisotropic potential problems. *Computers*

& Structures, vol. 86, no. 15, pp. 1656-1671.

Zhang, J.M; Yao, Z. (2001): Meshless regular hybrid boundary node method. *CMES- Computer Modeling in Engineering and Sciences*, vol. 2, no. 3, pp. 307-318.

Zhang, J.M.; Tanaka, M.; Matsumoto, T. (2004): Meshless analysis of potential problems in three dimensions with the hybrid boundary node method. *International Journal for numerical methods in Engineering*, vol. 59, no. 9, pp. 1147-1160.

Zhang JM.; Qin XY.; Han X.; Li GY. (2009): A boundary face method for potential problems in three dimensions. *International Journal for Numerical Methods in Engineering*, vol 80, no.3, pp. 320–337.

Zhang YM.; Gu Y,; Chen JT. (2009): Boundary layer effect in BEM with high order geometry elements using transformation. *CMES- Computer Modeling in Engineering and Sciences*, vol. 45, no. 3, pp. 227-247.

Zhang, Y.; Gu, Y.; Chen, J. T. (2010): Boundary element analysis of the thermal behaviour in thin-coated cutting tools. *Engineering Analysis with Boundary Elements*, vol. 34, no. 9, pp. 775-784**.**